ROYAL SOCIETY OF CHEMISTRY

PAPER

CrossMark
click for updates

A triboelectric textile templated by a three-dimensionally penetrated fabric†

Lianmei Liu,‡[a] Jian Pan,‡[b] Peining Chen,[b] Jing Zhang,[b] Xinghai Yu,[b] Xin Ding,*[a] Bingjie Wang,[b] Xuemei Sun[b] and Huisheng Peng*[b]

Commercially available 3D spacer fabrics with a three-dimensionally penetrated structure are directly coated with PDMS to fabricate triboelectric textiles without a multilayer structure and metal materials. The resulting triboelectric textile with a size of 5×5 cm^2 and a thickness of 8 mm generates an open-circuit voltage up to -500 V and a short-circuit current amplitude of 20 μA, corresponding to a peak power density of 153.8 mW m^{-2} at a load resistance of 1 GΩ. In addition, the performance of the triboelectric textile depends on its thickness, area, the frequency and force of pressing and remains stable after pressing and releasing for over 3000 cycles. Besides, in order to prove that the triboelectric textile is a reliable power source, a LCD and 49 LEDs lit up by a TET without any energy storage unit or rectification circuit have been exhibited apparently. The ingenious structure and simple fabrication are unique advantages of the triboelectric textile, which make it possible to realize practical applications and industrialization.

Introduction

The emergence of wearable electronic products such as e-skins, Google glasses, and Apple watches has opened a new technical revolution and may change our life in the near future. However, powering these promising devices remains a challenging and urgent task. The mainstream energy harvesting and storage systems typically appear as a rigid plate that is not flexible. Recently, these power systems have also been made into thin films to make them flexible. However, they could not be twisted three-dimensionally. In particular, the film structure cannot effectively satisfy the requirements of wearable electronic devices. To this end, a lot of efforts were made to explore fiber-shaped solar cells that can further form textiles to generate electric energy.[1–4] Unfortunately, the photovoltaic performances of solar cell textiles strongly depend on weather conditions and are not stable under some conditions; they may work only at day time and cannot generate power at night; it is necessary to

fabricate them with relatively high costs and low efficiencies in many applications.

As a newly appearing power source, triboelectric generators have been developed to produce electric energy due to the combined effect of contact electrification and electrostatic induction.[5–7] A variety of structural configurations, ranging from stacked polymer and metal layers[8–12] to rough surfaces[13–16] with high contact areas, were designed to fulfill the energy requirement of wearable electronic devices. Some devices have also been fabricated with springs to separate the top and bottom surfaces of the device.[17–19] Besides, there are also attempts to weave triboelectric generators into clothes,[20–27] though a complex and tedious fabrication process[17,28] was shared with high cost and low efficiency. Moreover, for the current triboelectric generators, a metal material like silver or aluminum[25,29–33] with a heavy weight is generally required for friction, and it is not compatible for wearable application.

In this article, a general and effective method is developed to fabricate novel flexible triboelectric textiles (TETs) based on commercially available fabrics with a three-dimensionally penetrated structure. They can efficiently convert mechanical energy from human motions like walking into electric energy. Unlike the previous reports[28,34] with spacers, springs or arched structures to separate the top and bottom surfaces of the device, the three-dimensionally penetrated structure of substrate textiles offers spontaneous elastic space for pressing and releasing. Beyond the structure of triboelectric nanogenerators, various holes on substrate textile surfaces spontaneously form rough poly(dimethylsiloxane) (PDMS) surfaces with many tiny pyramids, which can easily enhance their electrical output

[a] *Key Lab of Textile Science & Technology, Ministry of Education, State Key Laboratory for Modification of Chemical Fibers and Polymer Materials, College of Textiles, Donghua University, Shanghai 201020, China. E-mail: xding@dhu.edu.cn*

[b] *State Key Laboratory of Molecular Engineering of Polymers, Department of Macromolecular Science, Laboratory of Advanced Materials, Fudan University, Shanghai 200438, China. E-mail: penghs@fudan.edu.cn*

† Electronic supplementary information (ESI) available: Experimental techniques, SEM images of PET fabric, short-circuit current under different conditions and stability after being pressed for over 3000 cycles, and a triboelectric textile (TET) repeatedly pressed to light up forty-nine light-emitting diodes are included in Fig. S1 to S9 and Videos S1 and S2. See DOI: 10.1039/c6ta01166g

‡ These authors contributed equally to this work.

performance, instead of undergoing extra treatments (*e.g.*, plasma etching[35–37] or surface replication[38,39]) to obtain patterned surfaces. Therefore, the TET can be made through one step by dipping PDMS on the substrate textile, which is much simpler and easier than previous layer-by-layer methods. In addition, metal or metal oxides as electrodes or triboelectric materials are generally rigid, stuffy and unsuitable for flexible and portable applications. Under pressing, a peak power density of 153.8 mW m^{-2} with open-circuit voltage up to 500 V is generated, and a small TET with a size of 5 × 5 cm^2 is demonstrated to simultaneously power a LCD or 49 light-emitting diodes. The output power remains stable after pressing and releasing for over 3000 cycles.

Experimental section

Fabrication of TET

A PDMS silicone elastomer substrate (Sylgard 184, Dow Corning) was mixed with a curing agent (Sylgard 184, Dow Corning) at a ratio of 10 : 1. The following mixture was then treated under ultrasonication and vacuum to be more uniform and eliminate air, respectively. The PET fabrics were bought from Diwang Contexture Co. Ltd. and tailored into different sizes. The uncured PDMS mixture was carefully dipped onto one surface of the fabric to be fully immersed in PDMS, followed by curing at 80 °C for 60 min. A conductive silver paste was thus coated on one surface of the textile to serve as one electrode, while twenty layers of aligned CNT sheets were closely stacked onto the other surface of the treated fabric to serve as the other electrode. The preparation of the aligned CNT sheet had been reported previously.[4]

Characterization of TET

Photographs were taken with a digital camera (Nikon J1, Tokyo, Japan). Scanning electron microscopy images were recorded by using a Hitachi S-4800 operating at 1 kV, and the samples were prepared by coating a thin layer of gold prior to the observation. A pulse pressure force was applied by a pneumatic punch (MTS-200C-R). The short-circuit current and open-circuit voltage of the TET were measured by using a digital source meter (Keithley 2410).

Results and discussion

A typical fabrication of the TET is schematically illustrated in Fig. S1,† and it starts from a commercially available fabric. The fabric template displays a three-dimensionally penetrated structure with poly(ethylene terephthalate) (PET) fibers woven across the top surface and penetrated along the thickness. Therefore, the fabric is elastic in the thickness direction and could be reversibly compressed. The bottom surface of the fabric is then coated with a thin layer of polydimethylsiloxane
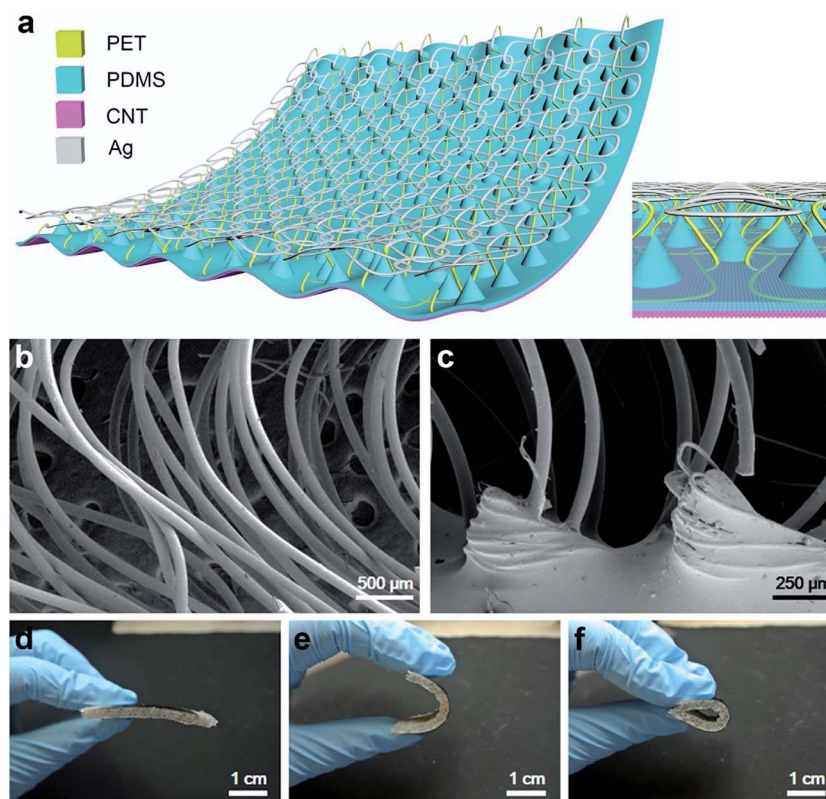
Fig. 1 (a) Schematic illustration of the structure of the TET. (b) and (c) SEM images of PET fibers in the fabric and pyramidal PDMS at the bottom surface of the fabric, respectively. (d–f) Photographs of a TET without bending (d) and being bent to 90° (e) and 180° (f). The TET showed a width of 5 cm and a thickness of 3 mm.
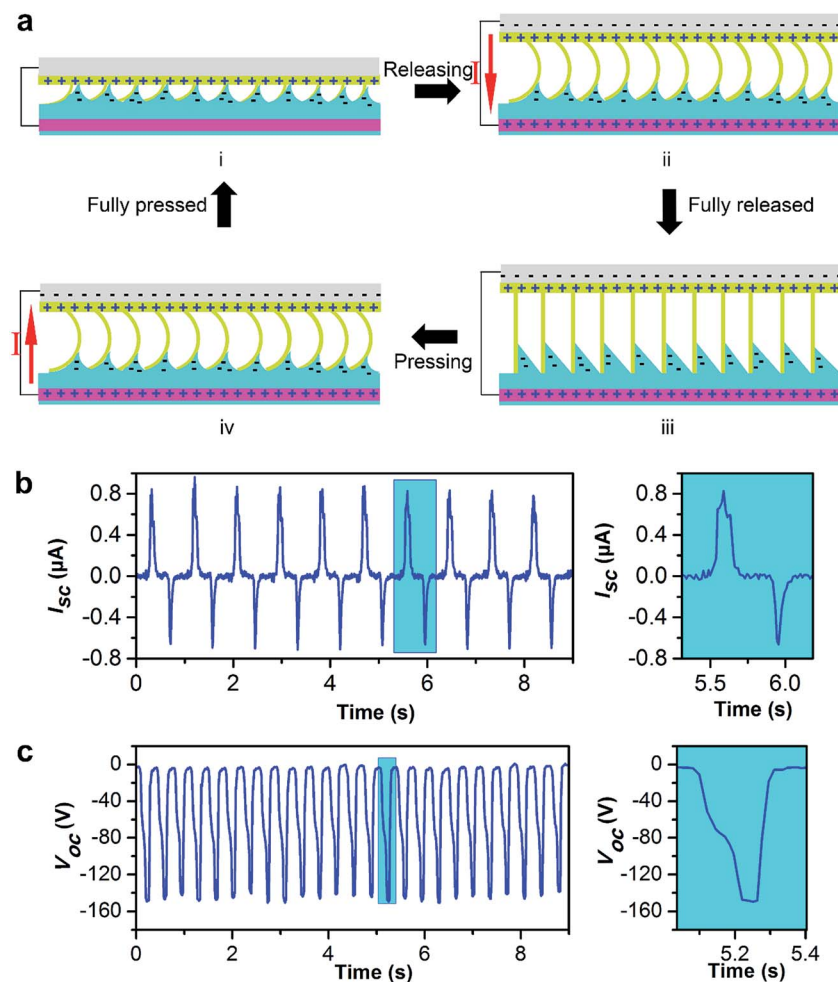
Fig. 2 (a) Schematic illustration of the electricity generation under pressing and releasing. (b) Short-circuit current with time (inset, one cycle). (c) Open-circuit voltage with time (inset, one cycle). The TET had a width of 5 cm and a thickness of 3 mm.

(PDMS) through a dip-coating process. A layer of silver paste and an aligned carbon nanotube (CNT) sheet are finally coated on the top and bottom surfaces as two electrodes to produce a TET (Fig. 1a), respectively.

The PET fibers were interlaced at the top surface of the fabric (Fig. S2a†) and aligned to penetrate across the thickness (Fig. 1b). PDMS can be infiltrated into the fabric due to the existence of large pores at a level of millimeters (Fig. S2b†). Interestingly, PDMS formed a large number of pyramids with sizes of hundreds of micrometers to millimeters at the bottom of the PET fabric. The PDMS pyramids were not penetrated through the textile due to the prevention of densely arranged PET fibers across the thickness direction (Fig. 1c and S10†), providing a rough surface for sufficient frictions against the PET fiber upon subjection to a pressure force (Fig. S3a†). The silver paste was deposited on the PET fibers at the top surface, and the modified PET fibers were cross-linked to serve as one electrode. The CNT sheet was dry-drawn from a spinnable CNT array synthesized by chemical vapor deposition, and the building CNTs were highly aligned along the same direction (Fig. S3b†). The aligned CNT sheet was flexible and can well maintain the structural integrity under bending; it was mechanically strong

(tensile strengths of 10^2 to 10^3 MPa) and electrically conductive (electrical conductivities of 10^2 to 10^3 S cm^{-1} at room temperature).[4] Therefore, it may function as the second electrode at the bottom. To further enhance the stability of the aligned CNT layer in the TET, another thin layer of PDMS was coated onto the paved CNT sheet. The designed structure makes the TET flexible and stable, and no obvious damage in the structure was detected after bending at an angle from 0° to 90° and 180° (Fig. 1d–f).

The mechanism for electricity generation is schematically depicted in Fig. 2a. No electric output is available at the original state where PDMS and PET were separated. Once a pressure force is applied on the TET, the PET fibers across the thickness direction bend to contact the PDMS pyramids at the bottom surface. PDMS is prone to bring electrons from PET because PDMS is more triboelectrically negative according to the triboelectric series.[5] Note that the opposite charges with an equivalent amount could be well maintained at each surface as both PET and PDMS are insulators. Upon removal of the applied pressure force, the PET fibers and PDMS rapidly separated from each other because of their high elasticity. To maintain an electric equilibrium of the system, during the releasing process,
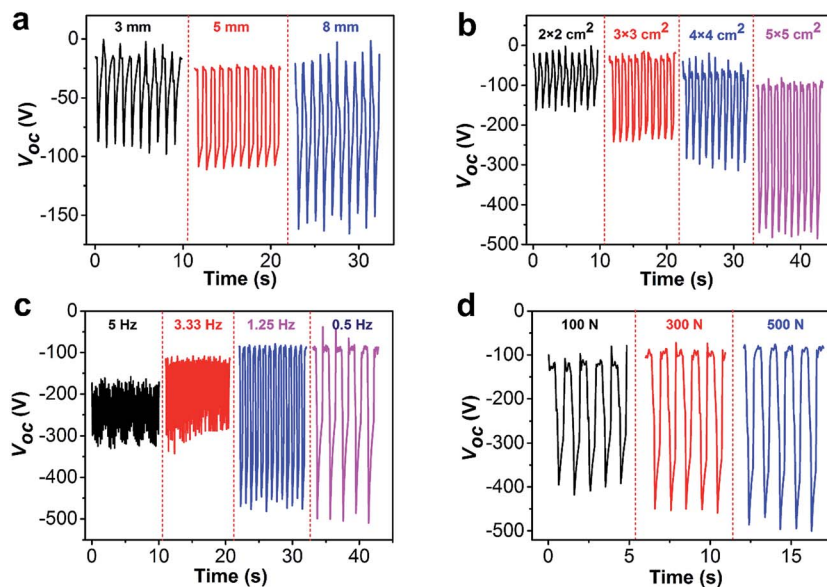
Fig. 3 (a) Open-circuit voltages at increasing thicknesses with the same size (2×2 cm^2). (b) Open-circuit voltages at increasing sizes with the same thickness (8 mm). (c) and (d) Open-circuit voltages at increasing pressing frequencies and forces, respectively. The TET had a thickness of 8 mm and a size of 5×5 cm^2 at (c and d).

the PET fibers with positive charges will induce equivalent negative charges on silver paste and meanwhile, PDMS with negative charges will induce positive charges on the CNT sheet. Consequently, electrons will flow to the silver paste electrode from the CNT sheet electrode through an external circuit and a negative current is generated (Fig. 2b).[14,40] The silver paste and CNT sheet electrodes will be negatively and positively charged with an equivalent value after fully releasing, respectively. As expected, an open-circuit voltage was produced as a result of the accumulation of negative charges on silver paste while positive charges on the CNT sheet (Fig. 2c). For instance, a negative voltage with a peak value of -150 V was generated by a TET with a size of 2×2 cm^2 upon a pressure force of 16 N per square centimeter. If a pressure force was subsequently applied on the textile, the electric equilibrium will be achieved again between the PET and PDMS due to contact with each other. As a result, the electrons at the silver paste electrode will flow back to the CNT sheet electrode to generate a positive current signal (Fig. 2b), accompanied by a decrease in electric potential difference as shown in Fig. 2c.

Note that the voltage did not start from zero in Fig. 2c because the textile could not fully return to the original state at a high pressing/releasing frequency. In contrast, the voltage started from zero when a relatively low pressing/releasing frequency was used (Fig. S4†). The electric signals could be repeatedly generated if a cyclic pressure force was applied upon the textile. The negative voltage was recorded during the operation as the PDMS was connected to the positive side of the voltmeter with the other surface being connected to the negative side.

The impact of thickness and size on the TET had been carefully investigated. The electric outputs were compared with increasing thicknesses of 3, 5 and 8 mm at the same size of 2×2 cm^2 (Fig. 3a). Upon application of the same pressure force and frequency of 64 N and 1 Hz, the generated voltages increased with increasing thickness. This phenomenon may be explained by the enhanced electrostatic induction in the thicker TET, i.e., more charges can be induced as the increased distance between the two surfaces provided more space for the separation of electrodes.

The voltage output could also be scaled up by using larger sizes of textiles. For instance, under the same conditions, enhanced voltages of -160 V, -240 V, -310 V and -480 V could be obtained by using the textiles with increasing sizes of 2×2 cm^2, 3×3 cm^2, 4×4 cm^2 and 5×5 cm^2, respectively (Fig. 3b). It was easy to understand that larger textiles with larger contact areas induced more charges, and higher voltages were thus generated. Similarly, the current outputs also increased with increasing sizes of textiles (Fig. S5†). The TET with a size of 5×5 cm^2 and a thickness of 8 mm was mainly demonstrated unless otherwise specified.

The magnitude and frequency of the pressure force also greatly affected the electric outputs of the TET. For instance, when the pressing frequency decreased from 5 to 0.5 Hz under the same applied force of 400 N, the voltages increased from -320 to -500 V (Fig. 3c). It was probably because the contacting and friction time between the two surfaces became longer under the pressure force with lower frequency, indicating that more charges and higher open-circuit voltages could be generated. In contrast, the two surfaces rapidly come into contact and separate at a higher frequency, so an insufficient electrification effect occurred with less charges and lower voltages. Similarly, lower current outputs were obtained under pressure forces with higher frequencies (Fig. S6†).

As expected, the electric outputs could also be enhanced by increasing the magnitude of pressure force (Fig. 3d). For

6080 | J. Mater. Chem. A, 2016, 4, 6077–6083

This journal is © The Royal Society of Chemistry 2016
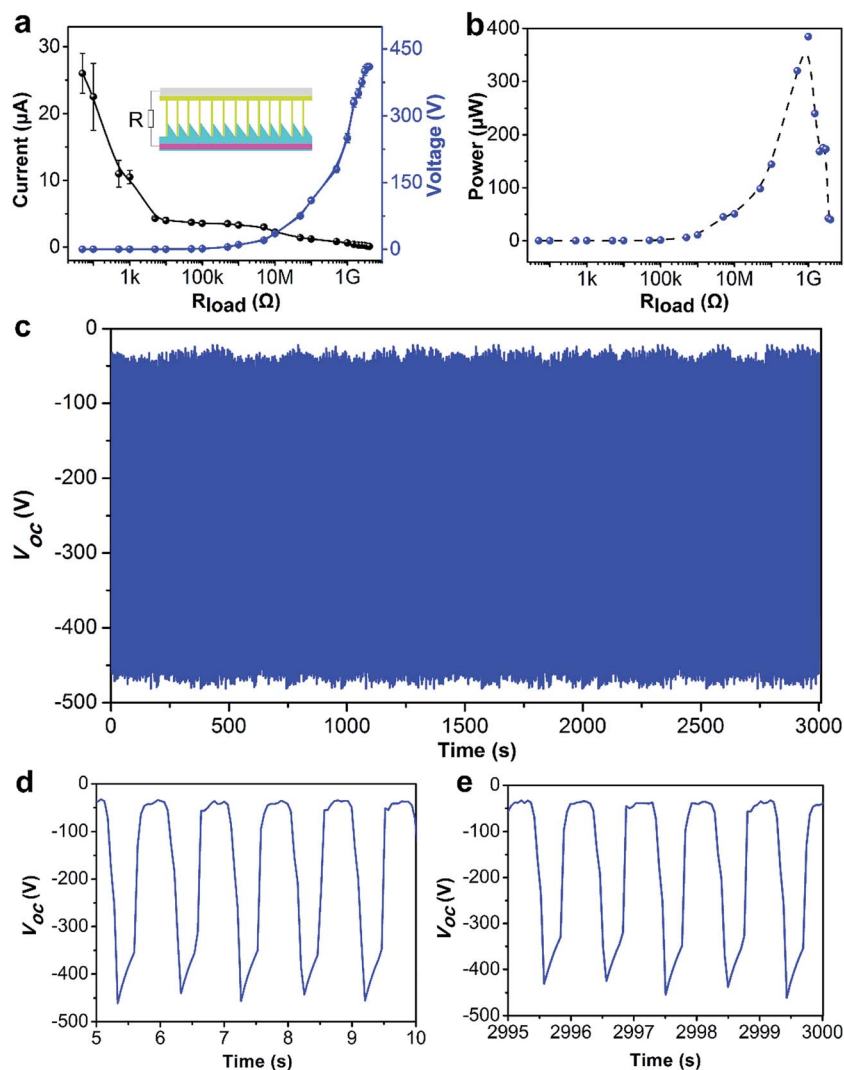
Fig. 4 (a) Dependence of output current and voltage on load resistance. (b) Dependence of power density on load resistance. (c) Cyclic reversibility on the output voltage. (d) and (e) Voltage outputs at the beginning and ending five cycles, respectively. The TET had a thickness of 8 mm and size of 5×5 cm^2, and the pressing frequency and force were 1 Hz and 400 N, respectively. For (a) to (e), the pressing frequency and force were 1 Hz and 400 N, respectively. The TET had a thickness of 8 mm and a size of 5×5 cm^2 at (a–e).

instance, increasing voltages from −400 to −500 V were generated with increasing forces from 100 to 600 N under the same other conditions. As expected, a similar dependence of force magnitude on the current outputs is also shown in Fig. S7.†

To better understand the TET as a power source, a TET with a thickness of 8 mm and a size of 5×5 cm^2 was connected by a load resistance in series to measure the voltage and current. The current output was found to reduce with increasing load resistance due to the ohmic loss (Fig. 4a). However, the voltage output showed an opposite trend under the same conditions. The instantaneous power output calculated by $W = I^2R$ (Fig. 4b) first increased and then decreased with increasing load resistance from nearly 100 Ω to 4 GΩ. A peak value of 384.4 µW or 153.8 mW m^{-2} occurred at 1 GΩ.

The electric power could be generated with a high reversibility. For instance, no obvious decrease in voltage output was found for over 3000 cycles of pressing and releasing (Fig. 4c). Fig. 4d and e further demonstrate that the voltage outputs were close during the 5–10th and 2995–3000th cycles. The reversibility in the performance was further verified by the fact that no obvious structural damage was observed for a TET after over 3000 cycles (Fig. S8†).

In order to illustrate the potential application of the TET as a power supply device, it was used to power a LCD. As shown in Fig. S9,† a LCD was connected with the TET directly. Firstly, when the TET was slightly pressed, a small voltage signal of nearly 200 mV was generated and the small image of a battery was shown on the LCD (Fig. 5a). Then, when the pressing force was increased to a fixed value, the voltage also increased from 1 V and was finally stable at 6 V, due to the accumulation of charges generated in PDMS and PET from contact electrification (Fig. 5b). As a result, the LCD was also lit partly at first and then completely (Video S1†). In addition, the TET was made into
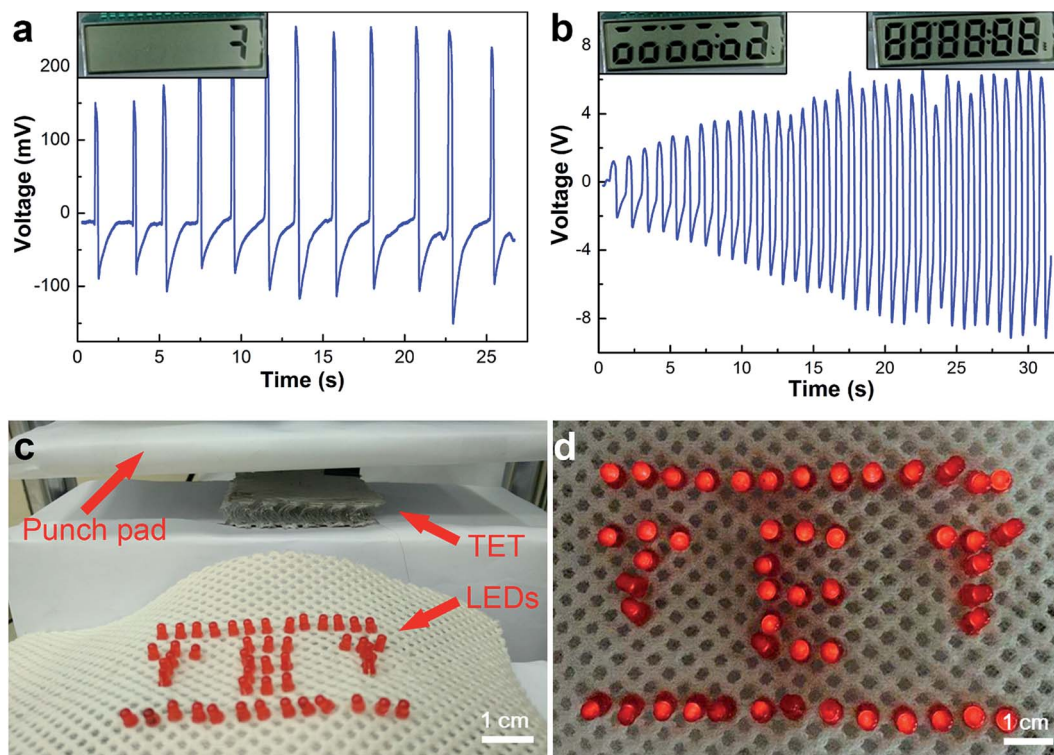
Fig. 5 (a) The voltages generated by pressing a TET slightly with a finger. The inset is the small image of a battery shown on the LCD. (b) The voltages generated by pressing a TET with a hand. The insets are the LCD lit partly and completely. (c) A TET put under a punch pad. (d) The TET at (c) being pressed to light up 49 light-emitting diodes. The TET had a thickness of 8 mm and a size of 5×5 cm^2, and the pressing frequency and force were 1 Hz and 400 N, respectively at (c) and (d).

an insole to convert mechanical energy to electricity to light up an LCD when walking (Fig. S11 and Video S3†).

A TET was also connected to power an array of 49 light-emitting diodes which were connected in series to form a pattern of "TET". The TET was placed under a press pad of a punch which supplied controllable presses (Fig. 5c). There were no any energy storage unit or rectifier in the circuit, therefore the LEDs were lit up directly by the generated electric signals from the TET. Fig. 5d presents the light-emitting diodes lit by pressing the TET with a force of 100 N at a frequency of 1 Hz. The 49 light-emitting diodes turned on and off with the periodic pressing and releasing (Video S2†). Besides, a 5×5 cm^2 TET could also be used to charge a common lithium ion battery with a capacity of 1200 mA h (Fig. S12†).

Conclusions

In summary, a new family of flexible triboelectric textiles is created from a commercially available PET fabric with a three-dimensionally penetrated structure through a neat solution process. These textile generators can efficiently convert mechanical energy into electric energy with an open-circuit voltage over 500 V and a maximal power density of 153.8 mW m^{-2}, which can drive a LCD or tens of LEDs. They are flexible, mechanically robust and low-cost, and can be widely used in wearable electronics. Based on the varied electric signals in response to environmental changes such as pressing, these

TETs can also be used as effective sensors to detect body movements in turn.

Notes and references

1 D. Zou, D. Wang, Z. Chu, Z. Lv and X. Fan, *Coord. Chem. Rev.*, 2010, **254**, 1169–1178.

2 T. Chen, L. Qiu, Z. Cai, F. Gong, Z. Yang, Z. Wang and H. Peng, *Nano Lett.*, 2012, **12**, 2568–2572.

3 L. Qiu, J. Deng, X. Lu, Z. Yang and H. Peng, *Angew. Chem., Int. Ed.*, 2014, **53**, 10425–10428.

4 Z. Zhang, K. Guo, Y. Li, X. Li, G. Guan, H. Li, Y. Luo, F. Zhao, Q. Zhang, B. Wei, Q. Pei and H. Peng, *Nat. Photonics*, 2015, **9**, 233–238.

5 Z. L. Wang, *ACS Nano*, 2013, 7, 9533–9557.

6 F. Hu, Q. Cai, F. Liao, M. Shao and S.-T. Lee, *Small*, 2015, **11**, 5611–5628.

7 S. Wang, L. Lin and Z. L. Wang, *Nano Energy*, 2014, **11**, 436–462.

8 P. Bai, G. Zhu, Z.-H. Lin, Q. Jing, J. Chen, G. Zhang, J. Ma and Z. L. Wang, *ACS Nano*, 2013, **7**, 3713–3719.

9 W. Yang, J. Chen, G. Zhu, J. Yang, P. Bai, Y. Su, Q. Jing, X. Cao and Z. L. Wang, *ACS Nano*, 2013, **7**, 11317–11324.

10 F. R. Fan, Z. Q. Tian and Z. L. Wang, *Nano Energy*, 2012, **1**, 328–334.

11 Y. H. Ko, G. Nagaraju and J. S. Yu, *RSC Adv.*, 2015, **5**, 6437–6442.

12 L. Yuan, X. Xu, T. Ding, J. Zhong, X. Zhang, S. Yue, B. Hu, Y. Huang, J. Zhou and Z. L. Wang, *Angew. Chem., Int. Ed.*, 2012, **124**, 4934–4938.

13 S. Wang, L. Lin and Z. L. Wang, *Nano Lett.*, 2012, **12**, 6339–6346.

14 G. Zhu, C. Pan, W. Guo, C. Y. Chen, Y. Zhou, R. Yu and Z. L. Wang, *Nano Lett.*, 2012, **12**, 4960–4965.

15 B. N. Chandrashekar, B. Deng, A. S. Smitha, Y. Chen, C. Tan, H. Zhang, H. Peng and Z. Liu, *Adv. Mater.*, 2015, **27**, 5210–5216.

16 F. R. Fan, L. Lin, G. Zhu, W. Wu, R. Zhang and Z. L. Wang, *Nano Lett.*, 2012, **12**, 3109–3114.

17 J. Chen, G. Zhu, W. Yang, Q. Jing, P. Bai, Y. Yang, T.-C. Hou and Z. L. Wang, *Adv. Mater.*, 2013, **25**, 6094–6099.

18 H. Guo, X. He, J. Zhong, Q. Zhong, Q. Leng, C. Hu, J. Chen, L. Tian, Y. Xi and J. Zhou, *J. Mater. Chem. A*, 2014, **2**, 2079–2087.

19 F. R. Fan, J. Luo, W. Tang, C. Li, C. Zhang, Z. Tian and Z. L. Wang, *J. Mater. Chem. A*, 2014, **2**, 13219–13225.

20 S. Jung, J. Lee, T. Hyeon, M. Lee and D. H. Kim, *Adv. Mater.*, 2014, **26**, 6329–6334.

21 T. C. Hou, Y. Yang, H. Zhang, J. Chen, L. J. Chen and Z. L. Wang, *Nano Energy*, 2013, **2**, 856–862.

22 T. Zhou, C. Zhang, C. B. Han, F. R. Fan, W. Tang and Z. L. Wang, *ACS Appl. Mater. Interfaces*, 2014, **6**, 14695–14701.

23 J. Wang, X. Li, Y. Zi, S. Wang, Z. Li, L. Zheng, F. Yi, S. Li and Z. L. Wang, *Adv. Mater.*, 2015, **27**, 4830–4836.

24 Y. H. Ko, G. Nagaraju and J. S. Yu, *RSC Adv.*, 2014, **5**, 6437–6442.

25 S. Lee, W. Ko, Y. Oh, J. Lee, G. Baek, Y. Lee, J. Sohn, S. Cha, J. Kim and J. Park, *Nano Energy*, 2015, **12**, 410–418.

26 K. N. Kim, J. Chun, J. W. Kim, K. Y. Lee, J.-U. Park, S.-W. Kim, Z. L. Wang and J. M. Baik, *ACS Nano*, 2015, **9**, 6394–6400.

27 J. Zhong, Y. Zhang, Q. Zhong, Q. Hu, B. Hu, Z. L. Wang and J. Zhou, *ACS Nano*, 2014, **8**, 6273–6280.

28 G. Zhu, Z. H. Lin, Q. Jing, P. Bai, C. Pan, Y. Yang, Y. Zhou and Z. L. Wang, *Nano Lett.*, 2013, **13**, 847–853.

29 S. Lee, J. Lee, W. Ko, S. Cha, J. Sohn, J. Kim, J. Park, Y. Park and J. Hong, *Nanoscale*, 2013, **5**, 9609–9614.

30 C. K. Jeong, K. I. Park, J. Ryu, G. T. Hwang and K. J. Lee, *Adv. Funct. Mater.*, 2014, **24**, 2620–2629.

31 K. I. Park, M. Lee, Y. Liu, S. Moon, G. T. Hwang, G. Zhu, J. E. Kim, S. O. Kim, D. K. Kim and Z. L. Wang, *Adv. Mater.*, 2012, **24**, 2999–3004.

32 Y. Yang, Y. S. Zhou, H. Zhang, Y. Liu, S. Lee and Z. L. Wang, *Adv. Mater.*, 2013, **25**, 6594–6601.

33 Q. Leng, H. Guo, X. He, G. Liu, Y. Kang, C. Hu and Y. Xi, *J. Mater. Chem. A*, 2014, **2**, 19427–19434.

34 M. Ha, J. Park, Y. Lee and H. Ko, *ACS Nano*, 2015, **9**, 3421–3427.

35 X. Wen, W. Yang, Q. Jing and Z. L. Wang, *ACS Nano*, 2014, **8**, 7405–7412.

36 G. Zhu, Y. Su, P. Bai, J. Chen, Q. Jing, W. Yang and Z. L. Wang, *ACS Nano*, 2014, **8**, 6031–6037.

37 L. Lin, Y. Xie, S. Niu, S. Wang, P.-K. Yang and Z. L. Wang, *ACS Nano*, 2015, **9**, 922–930.

38 S. Wang, L. Lin, Y. Xie, Q. Jing, S. Niu and Z. L. Wang, *Nano Lett.*, 2013, **13**, 2226–2233.

39 S. Wang, Y. Xie, S. Niu, L. Lin and Z. L. Wang, *Adv. Mater.*, 2014, **26**, 2818–2824.

40 C. Zhang, W. Tang, C. Han, F. Fan and Z. L. Wang, *Adv. Mater.*, 2014, **26**, 3580–3591.